ELSEVIER

Colloids and Surfaces A: Physicochem. Eng. Aspects 212 (2003) 123–134

COLLOIDS AND SURFACES A

www.elsevier.com/locate/colsurfa

Adsorption kinetics of $C_{10}E_4$ at the air–water interface: consider molecular interaction or reorientation

Ya-Chi Lee [a], Hwai-Shen Liu [a], Shi-Yow Lin [b,*]

[a] *Department of Chemical Engineering, National Taiwan University, 1 Roosevelt Road, Sec. 4, Taipei 106, Taiwan, ROC*

[b] *Chemical Engineering Department, National Taiwan University of Science and Technology, 43, Keelung Road, Sec. 4, Taipei 106, Taiwan, ROC*

Received 24 October 2001; accepted 3 June 2002

Abstract

The adsorption kinetics of $C_{10}E_4$ was studied using a video-enhanced pendant bubble tensiometer. Two dynamic processes were studied. The bubble was suddenly created and $C_{10}E_4$ adsorbs onto a freshly created interface. After it had reached the equilibrium, the bubble was then impulsively shrunk and the surface was compressed with some change of area large enough to appreciably enrich the surface concentration and change the surface tension. Two sets of equilibrium data, equilibrium surface tension $\gamma(C_\infty)$ and surface equation of state $\gamma(\Gamma)$ were measured and utilized for the determination of model parameters. The data were analyzed by either considering the molecular interaction between the adsorbed molecules or assuming that surfactant molecules adsorb at interface in two orientation states. Both models fit the equilibrium $\gamma(C_\infty)$ and dynamic $\gamma(t)$ data well. There exists a shift on the control mechanism for $C_{10}E_4$ onto a freshly created air–water interface: diffusion-control at dilute C_∞ and mixed-control at higher C_∞. The re-equilibration for $C_{10}E_4$ out of a suddenly compressed surface at $C_\infty = 1.0 \times 10^{-8}$ mol cm^{-3} is also a mixed controlled process. An average diffusivity of $(7.2 \pm 1.0) \times 10^{-6}$ cm^2 s^{-1} and adsorption/desorption rate constants ($\beta_1 = 3.0 \times 10^7$ cm^3 (mol s)$^{-1}$ and $\alpha_1 = 5.1 \times 10^{-2}$ s)$^{-1}$ are obtained using the Frumkin model. A discussion on the effect of interfacial curvature of fluid/liquid interface was also provided.

Keywords: Adsorption kinetics; Diffusion; Equation of state; Reorientation; Surface tension

1. Introduction

The adsorption kinetics of nonionic polyoxyethylene surfactant, C_mE_n, has attracted many attentions since it is widely utilized in many industrial processes. It has been reported that there exists a strong molecular interaction between the adsorbed C_mE_n molecules. Therefore the Langmuir adsorption isotherm, which assumes no molecular interaction, fails to describe the adsorption behavior of C_mE_n.

Diamant and Andelman formulated the governing equations for a diffusion-controlled process with the consideration of molecular interaction

* Corresponding author. Tel.: +886-2-2737-6648; fax: +886-2-2737-6644

E-mail address: ling@ch.ntust.edu.tw (S.-Y. Lin).

0927-7757/02/$ - see front matter
PII: S0927-7757(02)00330-8

from a free energy point view [1,2]. Liggieri et al. proposed that the interfacial potential barrier should be taken into account for the adsorption process and a different time-dependent boundary condition was considered [3,4]. Eastoe et al. studied the dynamic surface tension for $C_{10}E_4$ by utilizing the maximum bubble pressure method and the dynamic data were analyzed using the short and long time approximation [5]. It is speculated that $C_{10}E_4$ obeys a diffusion-control adsorption at the beginning of the adsorption process, but turns to be mixed diffusive-kinetic at the end of adsorption process.

Miller et al. [6] proposed that non-instantaneous reorientation can result in acceleration or deceleration of surface tension changes as compared to a simple Langmuir model. A re-orientation model, which considers the change in the partial molar area with increasing surface pressure due to molecular orientation, has also been proposed to describe the non-ideal adsorption behavior of alkyl dimethyl phosphine oxide at liquid interfaces [7,8].

The aim of this work is to investigate the adsorption mechanism of $C_{10}E_4$ and to examine the possibility of reorientation of $C_{10}E_4$ molecules in the adsorbed layer. The adsorption behavior of $C_{10}E_4$ onto a freshly created and an impulsively expanded air–water interface at 25 °C was measured by using a video-enhanced pendant bubble tensiometer. Two models (the Frumkin and reorientation models) are applied to describe the equilibrium and dynamic data of surface tension. The experimental equation of state data (γ vs. Γ/Γ_{ref}) are utilized, working with the equilibrium surface tension (γ vs. ln C) data, to help on the determination of model parameters.

Pendant bubbles have nearly spherical fluid interfaces. It is more reasonable to simulate the mass transport problem approximately with a spherical interface than a planar one. The dynamic surface tension $\gamma(t)$ profiles were fitted with the theoretical curves predicted from: (i) the Frumkin model with a spherical fluid interface having a radius of curvature of 1 mm; and (ii) the reorientation mode with a planar interface. The curvature effect on adsorption kinetics of $C_{10}E_4$ is therefore discussed at the end of this work.

2. Experimental measurements

2.1. Materials

Nonionic surfactant $C_{10}E_4$ (Decyl tetraethylene glycol ether, $C_{10}H_{21}(OCH_2CH_2)_4OH$, purity > 99%) purchased from Nikko (Tokyo, Japan) was used without further modification. Aqueous solutions are prepared with clean water purified via a Barnstead NANOpure water purification system, with the output water having a specific conductance of less than 0.057 $\mu\Omega^{-1}$ cm^{-1}.

2.2. Cloud point

The cloud point of aqueous $C_{10}E_4$ solutions was measured by a dynamic light scattering (DLS) technique. Solutions are prepared in flasks and placed in a water thermostat with temperature stability $\pm$0.1 K for several days to allow the system to reach equilibrium. During the equilibration process, the samples are stirred at 200 rpm several times to ensure through mixing. After equilibrium is reached, the samples are moved to the sample tubes for the DLS measurement. The cloud point is determined from the turning point of the profile of dimensionless scattered light intensity (I/I_{Bz}) versus temperature [9]. Here I_{Bz} is the scattered light intensity for benzene at the same measurement condition.

2.3. Apparatus

A pendant bubble tensiometer enhanced by video digitization was employed for the measurement of dynamic surface tension $\gamma(t)$, equilibrium surface tension $\gamma(C)$ and equation of state $\gamma(\Gamma)$ of $C_{10}E_4$. The apparatus and the edge detection routine have been described in detail in previous studies [10,11]. The temperature variation of aqueous solution is less than $\pm$0.05 K [11]. A 17-gauge stainless steel inverted needle (1.07 mm i.d.; 1.47 mm o.d.) was used for the bubble generation.

2.4. Adsorption

A pendant bubble of air with a diameter of ca. 2 mm was formed in a $C_{10}E_4$ solution, which was

put in a quartz cell. Digital images of the bubble were taken sequentially and then processed to determine the surface area and surface tension. The time required to create an air bubble in this work is about 1.44 s, therefore a 0.72 s (half of the formation time) is added in order to evaluate a more accurate surface age.

The measurement was performed at 25 ± 0.1 °C for 23 different bulk concentrations ($2.0 \times 10^{-10} \sim 1.0 \times 10^{-6}$ mol cm^{-3}), and each sample was repeated 3–5 times. The bubbles were measured up to around $1 \sim 3$ h, depending on $C_{10}E_4$ concentration.

2.5. Impulsively deformed bubble

To study the re-equilibration of a rapidly compressed interface, air is allowed to leave the bubble through a solenoid valve to change the surface area abruptly (within 0.13 s) by ca. 20%. The solenoid valve is open for 0.07 s and the bubble is left to re-equilibrate (over hundreds of seconds). Bubble images are recorded during the shrinkage of bubble, and after the solenoid valve has been closed. The compression of the bubble interface increases the surface concentration, causing surfactants to desorb to restore equilibrium, typically over several hundred seconds. The relaxation of surface tension to restore equilibrium is monitored via the sequential digital images.

Two different bulk concentrations, $C_\infty = 1.0$ and 2.0 (10^{-8} mol cm^{-3}), were chosen for the experiment of surface expansion. At each concentration, the experiments were performed several times. Bubble images were processed after the runs to obtain the surface tension evolution (γ) and surface area (A).

2.6. Surface expansion

When the adsorption has reached the equilibrium state, the air–water interface was expanded and sequential digital images of the bubble are taken. At each working concentration (1.0 and 2.0×10^{-8} mol cm^{-3}), it was repeated for around ten times with expansion rate $dA/dt = 4.6$–17.3 mm^2 s^{-1}. From the dynamic data of surface area $A(t)$, dA/dt and $\gamma(t)$, the dependences of γ vs. t and γ vs. A were obtained. A unique dependence between γ and A/A_{ref} (relative surface area) for those runs with large dA/dt was obtained [12]. This implies there is nearly no surfactant molecule adsorbing onto the expanding surface during this process at large expansion rate. A unique curve relating γ and Γ/Γ_{ref} (relative surface concentration), i.e. the equation of state, are then obtained and utilized on the determination of adsorption isotherm and model parameters.

2.7. Surface tension

The edge coordinates of pendant bubble are best fitted with the theoretical shape generated from the classical Laplace equation. The accuracy and reproducibility of the γ measurements are ca. 0.1 mN m^{-1} [10].

3. Theoretical framework

The mass transport of $C_{10}E_4$ molecules from aqueous bulk phase onto the interface of a freshly created and an impulsively expanded pendant bubble in a quiescent surfactant solution is modeled. Two approaches are considered: (i) the Frumkin model with the consideration of molecular interaction between the adsorbed $C_{10}E_4$ molecules; and (ii) reorientation model which assumes that $C_{10}E_4$ can adsorb in two orientation states with different partial molar area. $C_{10}E_4$ is assumed not to dissolve into the gas phase of the bubble and the convection effect is negligible.

3.1. Case I. Frumkin Model

In this approach, the mass transport in bulk is considered to be a 1-D diffusion onto a spherical surface. Bulk diffusion is considered to be spherical symmetric. A modified Ward and Tordai's equation results from Ref. [10]:

$$\Gamma(t) = \Gamma_b + (D/b)\left[C_\infty t - \int_0^t C_s(\tau)\,\mathrm{d}\tau\right] + 2(D/\pi)^{1/2} \times \left[C_\infty t^{1/2} - \int_0^{\sqrt{t}} C_s(t-\tau)\,\mathrm{d}\tau^{1/2}\right] \quad (1)$$

where D denotes the diffusivity, $C_s(t)$ is the subsurface concentration, $\Gamma(t)$ is the surface concentration, Γ_b is the initial surface concentration, b is the bubble radius, and C_∞ is the bulk concentration far from the bubble surface.

The adsorption equation used here utilizes the Langmuir formalism and assumes that the rate of mass transport across the interface depends upon the activation energies of the adsorption and desorption processes [13]. The activation energies are proportional to surface concentration Γ ($E_a = E_a^0 + v_a\Gamma RT/\Gamma_\infty$ and $E_d = E_d^0 + v_d\Gamma RT/\Gamma_\infty$ with constants E_a^0, E_d^0, v_a and v_d).

$$\mathrm{d}\Gamma/\mathrm{d}t = \beta_1 \exp(-v_a\Gamma/\Gamma_\infty)C_s(\Gamma_\infty - \Gamma) - \alpha_1 \exp(-v_d\Gamma/\Gamma_\infty)\Gamma \quad (2)$$

$$\frac{\Gamma}{\Gamma_\infty} = x = \frac{C_\infty}{C_\infty + a\exp(Kx)} \quad (3)$$

where β_1 and α_1 are the rate constant of adsorption and desorption processes, T is the temperature, R is the gas constant. Γ_∞ (the maximum surface concentration), K ($= v_a - v_d$) and a are the parameters. Parameter K takes into account the molecular interaction between the adsorbed surfactants and a indicates the surfactant activity.

Eq. (3) becomes the Langmuir adsorption isotherm when E_a and E_d are independent on Γ (i.e. $v_a = v_d = 0$). The presence of cohesive intermolecular forces, which lower the desorption rate at increasing Γ, is described by $K < 0$ [14–17]. Alcohols with long hydrocarbon chains are found to have a cooperative adsorption. A positive K indicates an anti-cooperative adsorption, which the adsorption becomes more difficult at increasing Γ [18–20].

For an ideal solution, the Gibbs adsorption equation $\mathrm{d}\gamma = -\Gamma RT\,\mathrm{d}\ln C$ and the equilibrium isotherm (Eq. (3)) allow for the calculation of the surface tension:

$$\gamma - \gamma_0 = \Gamma_\infty RT[\ln(1-x) - Kx^2/2] \quad (4)$$

where γ_0 is the surface tension of pure water. By fitting the data of $\gamma(C_\infty)$ and of $\gamma(\Gamma)$, the equilibrium constants (K, a and the maximum coverage Γ_∞) result.

When the adsorption process is controlled solely by bulk diffusion, the surface concentration can be obtained by solving Eqs. (1) and (3). If the adsorption process is of mixed control, Eq. (2) instead of Eq. (3) is solved coupled with Eq. (1) to find out the surface concentration. Then the dynamic surface tension $\gamma(t)$ was calculated from Eq. (4). In this work, it is assumed $v_a = 0$.

3.2. Case II. Reorientation model

Since the only available software package [21] restricted to planar interfaces, it is considered only the case of 1-D diffusion and adsorption onto a planar surface from a uniform bulk phase. The Ward and Tordai equation and the adsorption isotherms have been described in detail in previous studies [6,21,22]. The result of the theoretical model is the following integral equation:

$$\Gamma(t) = 2(D/\pi)^{1/2}\left[C_\infty t^{1/2} - \int_0^{\sqrt{t}} C_s(t-\tau)\,\mathrm{d}\tau^{1/2}\right] \quad (5)$$

Together with the respective adsorption isotherm, a complete set of equations was obtained to describe the adsorption process [21].

The adsorption isotherm for surfactant molecules which can adsorb in two states (1 and 2) with different partial molar area ω_1 and ω_2 ($\omega_1 > \omega_2$) can be expressed as [6,7,22]

$$C_\infty/a = \Gamma_2\omega/[1-\Gamma\omega]^{\omega_2/\omega} \quad (6)$$

$$-\Pi\omega/RT = \ln(1-\Gamma\omega) \quad (7)$$

where a is the adsorption equilibrium constant and ω is calculated from the following equations:

$$\Gamma = \Gamma_1 + \Gamma_2 \quad (8)$$

$$\omega\Gamma = \omega_1\Gamma_1 + \omega_2\Gamma_2 \quad (9)$$

$$\Gamma_1/\Gamma_2 = (\omega_1/\omega_2)\exp[(\omega_1 - \omega_2)/\omega]\exp[-\Pi(\omega_1 - \omega_2)/RT] \quad (10)$$

The model parameters are ω_1, ω_2 (molar areas

of molecules in state 1 and 2 in the adsorbed monolayer), a and α.

4. Experimental results

4.1. Cloud point

The cloud point (T_c) of surfactant solutions depends upon bulk concentration. It was reported that $T_c = 21.2$ °C for aqueous $C_{10}E_4$ solution at 1 wt.% concentration [23]. The variation of T_c for $C_{10}E_4$ around cmc was measured and shown in Fig. 1. At concentration close to cmc, the cloud point increases dramatically when $C_{10}E_4$ concentration decreases. The cmc of $C_{10}E_4$ at 25 °C is 6.8×10^{-7} mol cm^{-3} and $T_c = 27.5 \pm 0.1$ °C for $C_\infty = 7.01 \times 10^{-7}$ mol cm^{-3}. Surface tension measurements were done at 25 °C in this work. All solutions ($C_\infty <$ cmc) for the dynamic surface tension measurement in this work are therefore confirmed to be homogenous.

4.2. Fresh surface

Dynamic surface tension for the adsorption of $C_{10}E_4$ onto a clean air–water interface was measured up to 1–3 h from the moment (referenced as $t = 0$) at which one-half of the bubble volume is generated during the bubble formation. Shown in Fig. 2 are representative dynamic surface tension profiles (for one selected bubble at each bulk concentration) of solutions at nine different concentrations, $C_\infty = 0.13$, 0.35, 0.50, 0.75, 1.3, 2.0, 3.5, 6.0, and 10.0 (10^{-8} mol cm^{-3}). The reproducibility of $\gamma(t)$ is demonstrated later in Fig. 8. The equilibrium surface tension was extracted from the long time asymptotes for each concentration and shown in Fig. 3. Data in Fig. 2 also indicates that a complete dynamic profile for $C_{10}E_4$ solutions is available for $C_\infty < 3.5 \times 10^{-8}$ mol cm^3. At more elevated bulk concentration, the first γ data point is much lower than 72 mN m^{-1}. This implies the surface concentration at $t = 0.72$ s is already significant.

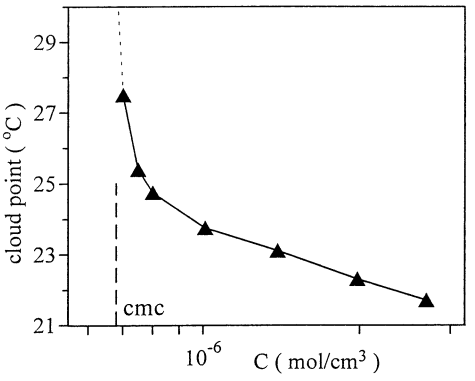

Fig. 1. The cloud point as a function of bulk concentration of $C_{10}E_4$.

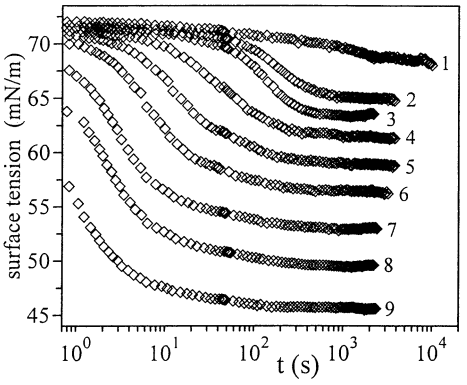

Fig. 2. Representative dynamic surface tensions for adsorption of $C_{10}E_4$ onto a clean air–water interface for C_∞ = (1) 0.13, (2) 0.35, (3) 0.50, (4) 0.75, (5) 1.3, (6) 2.0, (7) 3.5, (8) 6.0, and (9) 10.0 (10^{-8} mol cm^{-3}).

4.3. Compressed surface

Consider next the desorption of $C_{10}E_4$ out of an overcrowded surface caused by an impulsive shrinkage of the bubble. In Fig. 4(a), representative profiles of surface tension (circles) and surface area (triangles) obtained for a pendant bubble in a surfactant solution of $C_\infty = 1.0 \times 10^{-8}$ mol cm^{-3} are shown. In this example, the surface tension decreased from 60.55 mN m^{-1} (point A) down to 55.94 mN m^{-1} (point L) in 0.083 s. Thereafter, surfactant desorbs to re-establish equilibrium over roughly 500 s. The surface area of pendant bubble decreased 21% during the shrinkage and then kept a nearly constant value. All the relaxation data showed a similar behavior. The surface tension

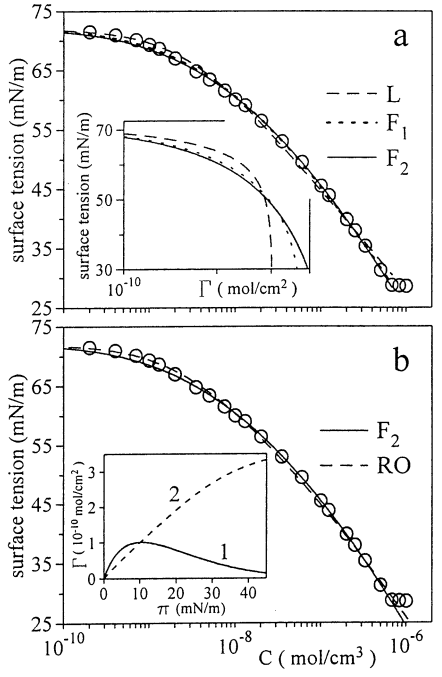

Fig. 3. Comparison between the experimental data and the profiles predicted from the (a) Langmuir (L), Frumkin (F_1 and F_2), and (b) reorientation (RO) adsorption isotherms. The insets shows (a) the model predictions relating surface tension and surface concentration and (b) the relaxations of surface concentration (Γ_1 and Γ_2) with surface area ω_1 (1) and ω_2 (2) as a function of surface pressure ($\gamma_0-\gamma$).

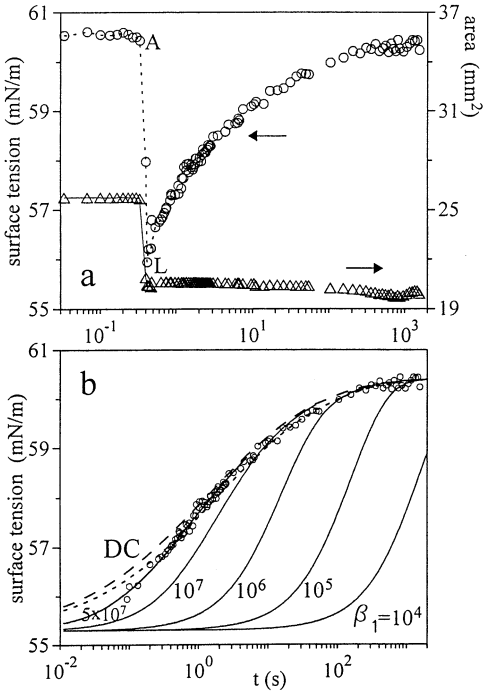

Fig. 4. (a) Representative dynamic surface tension and surface area of pendant bubble for the re-equilibration process due to a sudden compression of the interface for $C_\infty = 1.0 \times 10^{-8}$ mol cm^{-3} and (b) dynamic surface tension and theoretical predictions of diffusion-controlled (dashed curves) and mixed-controlled (solid curves) re-equilibration of the Frumkin (F_2) model. The dotted curve is the diffusion-controlled profile with $D = 4.0 \times 10^{-6}$ cm^2 s^{-1}. β_1 [=] cm^3 mol^{-1} s^{-1}.

decreased in about 0.1 s from the equilibrium value to a lower one, corresponding to the end of bubble shrinkage, and then increased smoothly up to its equilibrium value.

Table 1 presents a set of surface properties during the bubble shrinkage. The column of $A_i\Gamma_i/A_e\Gamma_e$ shows the relative amount of $C_{10}E_4$ molecules at surface from the experimental dependence of surface equation of state. The data indicate that adsorption took place during the ramp type area change. At $t = 5/60$ s, there are already 4.6% of surfactant molecules leaves the surface. This is why point A instead of point L was set as the initial time for the re-equilibration process.

The data in Fig. 4(a) were re-plotted in Fig. 4(b), with plotting the point A as $t = 0$ for the re-equilibration process. The initial surface concentration for these simulations was calculated from the mass balance, surface equation of state, and Eq. (4), $A_i\Gamma_i/A_e\Gamma_e$ and $\gamma_i(\Gamma_i)$. It was found that $\gamma = 55.3$ mN m^{-1} for keeping $A_i\Gamma_i/A_e\Gamma_e = 1.0$ at point L with the measured surface area, therefore it was set $\gamma = 55.3$ mN m^{-1} at $t = 0$ for the theoretical simulation of desorption. Note that a same controlling mechanism and nearly same rate constants resulted when the lowest surface tension (point L) was set as the initial point of the desorption process, as Ref. [19].

4.4. Expansion

Surface expansion experiment was performed using the pendant bubble technique to obtain the surface equation of state $\gamma(\Gamma)$ for $C_{10}E_4$. The pendent bubble, at which the interface has reached its equilibrium state, was expanded with different

Table 1
Relaxations of surface properties during the shrinkage of bubble, $C = 1 \times 10^{-8}$ mol cm^{-3}

t (s)	γ (mN m^{-1})	A (mm^2)	A_i/A_e	$\Gamma_i/\Gamma_{\gamma=62}$[a]	$A_i\Gamma_i/A_e\Gamma_e$[a]
−1/30	60.50	25.74	1.00	1.105	1.00
0	60.43[b]	25.68	1.00	1.110	1.00
2/30	57.97[c]	20.90	0.81	1.248	0.92
5/60	55.94[d]	20.45	0.79	1.325	0.95
3/30	56.20	20.41	0.79	1.317	0.95

[a] The relative surface concentration calculated from γ by applying the relationship of γ vs. $\Gamma/\Gamma_{\gamma=62}$, which was obtained from the fast expansion of pendant bubble.
[b] The point right before the desorption process, corresponding to the equilibrium state.
[c] The point during the shrinkage of bubble.
[d] The point with the lowest surface tension, corresponding to the end of shrinkage.

expansion rates dA/dt. A representative set of experimental data, $\gamma(t)$ and $A(t)$ during the expansion process, for $C_\infty = 1.0 \times 10^{-8}$ mol cm^{-3} is shown in Fig. 5.

During the expansion, the surface area of pendant bubble increases, for example from 20 to 33 mm^2 for the run of $dA/dt = 16$ mm^2 s^{-1} in 1.1 s, and depletes the surface concentration. The relaxation data in Fig. 5 are re-plotted in Fig. 6 to show the dependence of $\gamma(A/A_{ref})$. The data indicate as the expansion rate dA/dt is larger than 10 mm^2 s^{-1}, there exists a nearly unique $\gamma(A/A_{ref})$ relationship. The unique trend for the runs with different dA/dt implies that the amount of $C_{10}E_4$ molecules absorbs onto the air–water interface is negligible during this 1.2 s of surface expansion. The $\gamma(A/A_{\gamma=62\ mN\ m^{-1}})$ dependence for $dA/dt >$ 10 mm^2 s^{-1} is plotted in Fig. 7(b) showing the $\gamma(\Gamma/\Gamma_{\gamma=62\ mN\ m^{-1}})$ dependence, i.e. the equation of state of $C_{10}E_4$. The π $(=\gamma_0-\gamma)$ vs. A/A_{ref} dependence of $C_{10}E_4$ is shown in Fig. 7(a).

Expansion experiments were performed at two $C_{10}E_4$ concentrations: 1.0 and 2.0 (10^{-8} mol cm^{-3}). Shown in Fig. 7 is only that from 1.0×10^{-8} mol cm^{-3} since the expansion rate on $C_\infty = 2.0 \times 10^{-8}$ mol cm^{-3} in this work ($dA/dt = 6$–17 mm^2 s^{-1}) is not large enough to obtain a unique trend on $\gamma(\Gamma/\Gamma_{ref})$ or $\gamma(A/A_{ref})$ dependence.

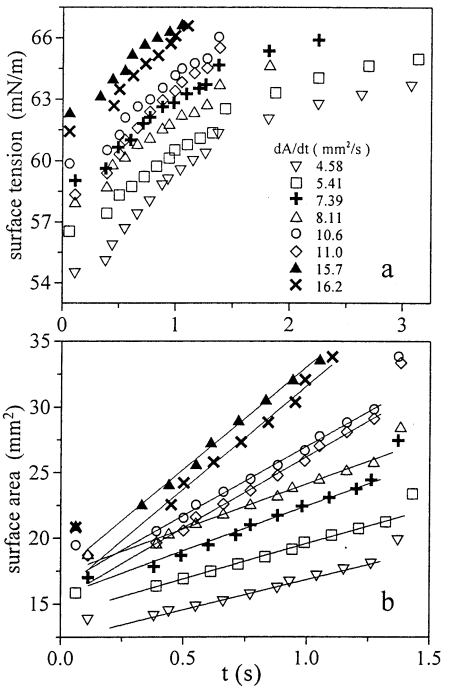

Fig. 5. Experimental data of (a) surface tension and (b) surface area A vs. time for the expansion experiment at $C_\infty = 1.0 \times 10^{-8}$ mol cm^{-3}. Each symbol represents a run at different expansion rate (dA/dt).

4.5. Case I. Frumkin model

Most previous studies on the determination of adsorption isotherm and the model constants applied only the data of equilibrium surface tension $\gamma(C_\infty)$. It has been proposed recently that a second set of equilibrium data $\gamma(\Gamma)$ is necessary on determining the adsorption isotherm and the parameters [12]. In this work, both sets of equilibrium data of $C_{10}E_4$ are applied.

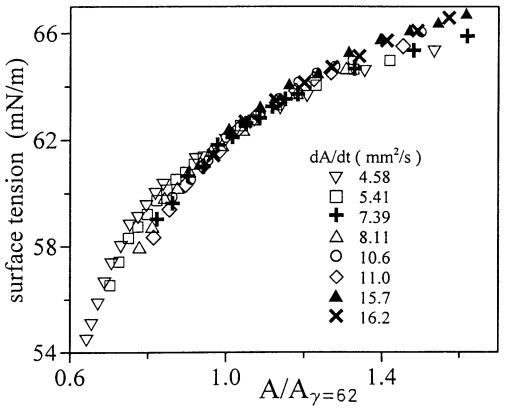

Fig. 6. Influence of expansion rate (dA/dt) on the relationship between surface tension and relative surface area (A/A_{ref}) for $C_\infty = 1.0 \times 10^{-8}$ mol cm^{-3}.

4.6. Equilibrium

Shown in Figs. 3 and 7 are the model predictions (solid curve F_2) which best-fit both $\gamma(C_\infty)$ and $\gamma(\Gamma)$ data. Shown in these two figures are also two curves: dotted one (F_1, from Frumkin model) and dashed one (L, from Langmuir model), which are the best-fit results by taking only the $\gamma(C_\infty)$ data into consideration. The deviation between theoretical curves F_1 and F_2 on $\gamma(C_\infty)$ diagram (Fig. 3) is insignificant, however in the inset of Fig. 7(b), a clear deviation is shown between curves F_1 and F_2 at the region of low surface tension. The model constants for L, F_1 and F_2 are listed in Table 2. Note that even F_1 and F_2 on $\gamma(C_\infty)$ diagram are very close to each other, the fit on $\gamma(t)$ results different diffusivities (discussed later).

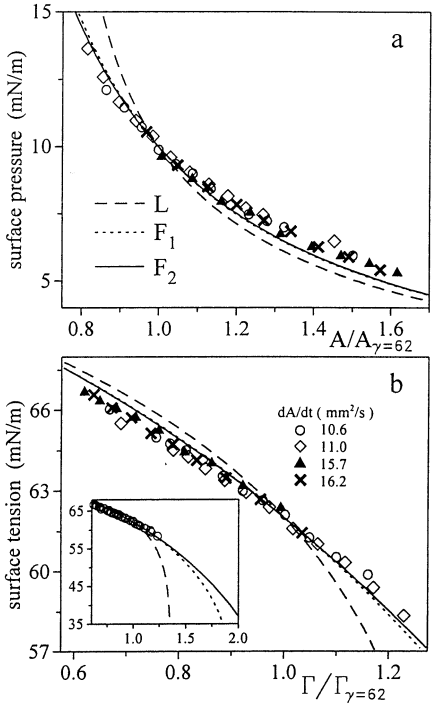

Fig. 7. Comparison between the experimental data and the profiles predicted from the Langmuir (L) and Frumkin (F_1 and F_2) models for surface pressure vs. relative surface area (a), and surface tension vs. relative surface concentration (b).

Both F_1 and F_2 predict a positive value of K (the parameter of molecular interaction). This indicates that the adsorption of $C_{10}E_4$ is anti-cooperative, i.e. the adsorption becomes more difficult as the surface coverage is higher. The Langmuir isotherm predicts poorly both $\gamma(C_\infty)$ and $\gamma(\Gamma)$ data. This poor prediction tells clearly that the molecular interaction between $C_{10}E_4$ molecules on adsorption process is significant and important.

The $\gamma(\Gamma/\Gamma_{ref})$ data in Fig. 7 do bring some (but not much) help on determining the model constants. Since the available $\gamma(\Gamma/\Gamma_{ref})$ dependence for $C_{10}E_4$ is restricted to $58 < \gamma < 67$ mN m^{-1}, the $\gamma(\Gamma/\Gamma_{ref})$ data in this work can't tell us precisely the optimal model constants.

4.7. Dynamic data

The dynamic $\gamma(t)$ data was fitted with the Frumkin model F_2 by assuming the adsorption process is of diffusion-control. A comparison between model predictions (the solid curves) and $\gamma(t)$ data for four concentrations, $C_\infty = 0.75$, 1.0, 1.3, and 2.0 (10^{-8} mol cm^{-3}) is shown in Fig. 8.

Table 2
Model constants of optimal fit of $C_{10}E_4$ aqueous solution

Model[a]	$\Gamma_\infty \times 10^{10}$ (mol cm^{-2})	$a \times 10^9$ (mol cm^{-3})	K
L[b]	3.02	2.68	
F_1[b]	3.80	1.75	2.86
F_2[c]	4.58	1.69	4.65

[a] L = Langmuir, F = Frumkin.
[b] Best-fit $\gamma(C)$ data.
[c] Best-fit both $\gamma(C)$ and $\gamma(\Gamma)$ data.

The Frumkin model predicts pretty well the dynamic data for all concentrations. A nearly constant diffusivity was resulted from the best-fit, as shown in Fig. 9. Note that the radius of curvature at apex of the pendant bubble is around 1 mm, therefore on the simulation it is assumed the air–water interface is spherical with radius of curvature of 1 mm. An average diffusivity of $(7.2\pm1.0)\times10^{-6}$ cm^2 s^{-1} (dashed line in Fig. 9) is resulted for $C_\infty < 3.5\times10^{-8}$ mol cm^{-3}. The adsorption of $C_{10}E_4$ onto a clean air–water interface at dilute concentrations is concluded to be a diffusion-controlled process.

Note that the diffusivity estimated from the Stokes–Einstein equation is $D_{AB}=kT/(6\pi R_A\mu_B)=4.7\times10^{-6}$ cm^2 s^{-1} [24]. Here k is the Boltzman's constant, T is temperature, R_A is the radius of spherical particle of molecules, and μ_B is the viscosity of the solvent. The radius of $C_{10}E_4$ molecules, R_A, is estimated from its volume per molecule ($V=4\pi R_A^3/3=M/\rho N$) with $M=$

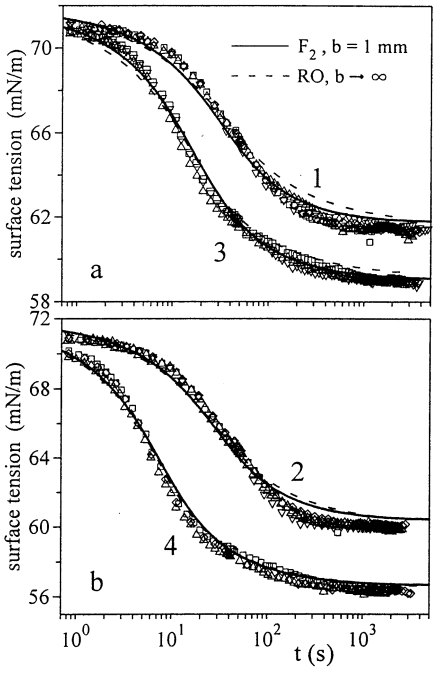

Fig. 8. Dynamic surface tensions of $C_{10}E_4$ and the theoretical diffusion-controlled profiles for Frumkin (F_2) and reorientation (RO) models at C_∞ = (1) 0.75, (2) 1.0, (3) 1.3, and (4) 2.0 (10^{-8} mol cm^{-3}).

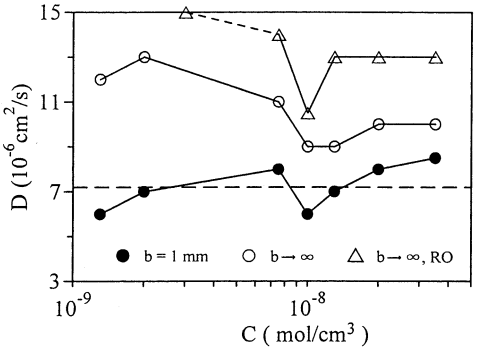

Fig. 9. Diffusivity (D) predicted from the reorientation (△) and Frumkin (○, ●) model as a function of bulk concentra-

molecular weight (334.5 g mol^{-1}), ρ = density (0.955 g cm^{-3} at 20 °C) of $C_{10}E_4$, and N is Avogadro's number. The diffusivity of a linear molecules and of a spherical one has been discussed by Hayduk and Buckley [25].

If the set of model parameter F_1 is applied to fit the dynamic $\gamma(t)$ data, the fit is nearly the same as F_2 does except now a slightly larger diffusivity $(7.7\pm1.5\times10^{-6}$ cm^2 s$^{-1})$ is resulted for $C_\infty < 3.5\times10^{-8}$ mol cm^{-3}.

The diffusion-controlled evolution of the surface tension for the re-equilibration process is shown in Fig. 4(b) as the dashed curve. The theoretical DC profile departs away from the dynamic $\gamma(t)$ data. Theoretical relaxation profiles with a finite adsorption rate constant (β_1) were also calculated and plotted (the solid curves). The fit clearly indicates that it is a diffusive-kinetic mixed diffusion controlled process. An adsorption rate constant $\beta_1=5.0\times10^7$ cm^3 (mol s)$^{-1}$ results from the fit.

As mentioned in Section 4, dynamic surface tension profiles for $C_{10}E_4$ solutions are incomplete $C_\infty > 3.5\times10^{-8}$ mol cm^{-3}, and therefore they are not used for evaluating the diffusivity. Fig. 10 illustrates a comparison between the dynamic data of $C_\infty=6.0\times10^{-8}$ mol cm^{-3} and the theoretical prediction of diffusion-control with $D=7.2\times10^{-6}$ cm^2 s^{-1} (from F_2 model). The dynamic data departs away from the diffusion-controlled curve and is concluded to be a mixed controlled process. The curve with $\beta_1=4.0\times10^7$ cm^3 (mol s)$^{-1}$ best-fit the dynamic $\gamma(t)$ data. However, if

one assumes that the adsorption is diffusion-controlled, the curve with $D = 5.5 \times 10^{-6}$ cm^2 s^{-1} (the dotted line) fits the dynamic $\gamma(t)$ data well. This lower diffusivity indicates the resistance of mass transport from the adsorption/desorption step is significant. Similar results (mixed-control and $\beta_1 = 4.0 \times 10^7$ cm^3 (mol s)$^{-1}$) are also observed from the dynamic $\gamma(t)$ data for $C_\infty = 1.0 \times 10^{-7}$ mol cm^{-3}.

The adsorption of $C_{10}E_4$ onto a freshly created air–water interface at $C_\infty = 6.0 \times 10^{-8}$ mol cm^{-3} and the desorption at $C_\infty = 1.0 \times 10^{-8}$ mol cm^{-3} out of a suddenly compressed surface are therefore concluded to be diffusive-kinetic mixed controlled process. In other words, $C_{10}E_4$ has a shift mechanism for the adsorption onto a fresh surface. Averaged values of the rate constants of adsorption and desorption are $\beta_1 = 4.3 \times 10^7$ cm^3 (mol s)$^{-1}$ and $\alpha_1 = 7.3 \times 10^{-2}$ s^{-1}.

4.8. Simulation

To confirm the mechanism of $C_{10}E_4$, a theoretical simulation was performed for the adsorption and desorption processes. The concentrations considered are 2×10^{-10}–7×10^{-7} mol cm^{-3}, in which the dynamic surface tension profiles are measured in this work. It is assumed that $v_a = 0$ and the effect of v_a has been discussed in previous articles [26,27].

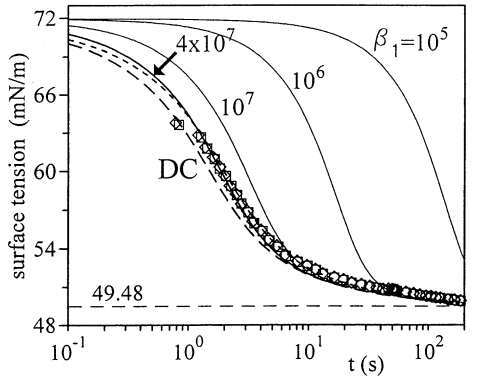

Fig. 10. A comparison between the dynamic data and the diffusion- (dashed curves) and mixed-controlled (solid curves) theoretical profiles for $C_\infty = 6.0 \times 10^{-8}$ mol cm^{-3} with $D = 7.2 \times 10^{-6}$ cm^2 s^{-1}. The dotted curve is the diffusion-controlled profile with $D = 5.5 \times 10^{-6}$ cm^2 s^{-1}. β_1 [=] cm^3 mol^{-1} s^{-1}.

The limiting adsorption rate constants β^l for the adsorption of $C_{10}E_4$ onto a clean interface and for the desorption out of a compressed surface are plotted in Fig. 11. The dashed horizontal line is the adsorption rate constant β_1 (4.3×10^7 cm^3 (mol s)$^{-1}$) obtained from experimental data. Fig. 11 confirms the previous conclusions. First, the adsorption at $C_\infty < 5 \times 10^{-8}$ mol cm^{-3} is diffusion controlled, whereas it is a mixed controlled process at higher C_∞. The re-equilibration process for $C_{10}E_4$ out of a suddenly compressed surface (with a 20% surface area decrease) is diffusion controlled at $C_\infty < 4 \times 10^{-9}$ mol cm^{-3} and is mixed controlled at higher C_∞. Therefore, the desorption run in this work at $C_\infty = 1.0 \times 10^{-8}$ mol cm^{-3} is a mixed controlled process.

4.9. Case II. Reorientation model

In this case, equilibrium $\gamma(C_\infty)$ was applied to determine the model parameters. The adsorption onto a freshly created air–water surface is assumed to be diffusion-controlled. Dynamic $\gamma(t)$ profiles are then used for the determination of diffusivity.

The parameters resulted from $\gamma(C_\infty)$ data are: $\omega_1 = 5.19 \times 10^9$ cm^2 mol^{-1}, $\omega_2 = 2.77 \times 10^9$ cm^2 mol^{-1}, $a = 6.11 \times 10^{-9}$ mol cm^{-3}, and $\alpha = 0.60$.

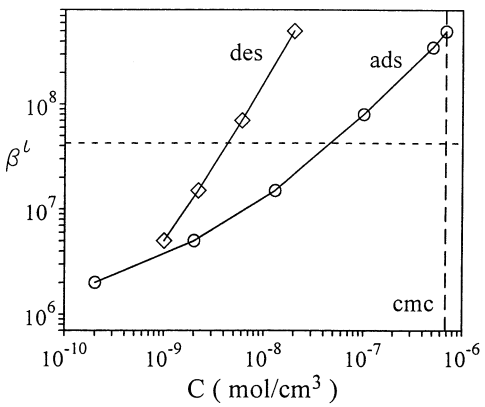

Fig. 11. The limiting adsorption rate constant β^l (cm^3 mol^{-1} s^{-1}) as a function of bulk concentration and adsorption rate constant β_1 (dashed line) of $C_{10}E_4$ resulted from the Frumkin (F_2) model with $D = 7.2 \times 10^{-6}$ cm^2 s^{-1} and $v_a = 0$.

The reorientation model describes the equilibrium $\gamma(C_\infty)$ perfectly and the dynamic $\gamma(t)$ data well, as shown in Figs. 3 and 8. However, the averaged diffusivity ($D = (13 \pm 1.3) \times 10^{-6}$ cm^2 s^{-1}, Fig. 9) resulted from the reorientation model and the Ward and Tardai's equation (with a planar interface) is much larger than that from the Frumkin model. The inset in Fig. 3(b) shows also the relaxations of surfactant concentration of $C_{10}E_4$ existing in different states (1 and 2) with molar area ω_1 and ω_2.

5. Discussion and conclusion.

Both the Frumkin and reorientation model can predict the equilibrium and dynamic surface tension profiles well. The equilibrium $\gamma(\Gamma)$ data help us on determining the model parameters. The adsorption of $C_{10}E_4$ molecules onto a freshly created interface is found to be anti-cooperative from the Frumkin model. This adsorption process at dilute surfactant concentrations is of diffusion control with $D = (7.2 \pm 1.0) \times 10^{-6}$ cm^2 s^{-1}. The controlling mechanism shifts to be mixed-controlled at higher concentration ($C_\infty > 5 \times 10^{-8}$ mol cm^{-3}). The re-equilibration process due to a sudden surface-compression is mixed controlled at $C_\infty > 4 \times 10^{-9}$ mol cm^{-3}. Rate constants of adsorption and desorption are $\beta_1 = 4.3 \times 10^7$ cm^3 (mol s)$^{-1}$ and $\alpha_1 = 7.3 \times 10^{-2}$ s^{-1}.

Lin et al. and Ferri et al. have reported that the effect of interfacial curvature on the study of adsorption kinetics is important [10,28,29]. The contribution on bulk diffusion due to the curvature of fluid interface is significant for small bubble or drop and/or at dilute concentration. Eq. (1) indicates that a higher surface concentration Γ results at the same t (adsorption time) for a bubble with a smaller b (radius). In other words, the dynamic adsorption profile relaxes faster for a spherical interface than a planar one. The theoretical profiles, assuming a planar bubble interface, fit the dynamic $\gamma(t)$ data satisfactorily, but is a little worse than the spherical surface with $b = 1$ mm. A representative example is shown in Fig. 12 for $C = 1.3 \times 10^{-8}$ mol cm^{-3}. A larger average-diffusivity results from the planar interface ($D = 10.6 \pm 1.5 \times 10^{-6}$ cm^2 s^{-1}, Fig. 9). Deviation on D is significant at dilute concentrations. A detailed study on the overestimation of diffusivity as a function of surfactant concentration and the curvature of interface is in process in our laboratory.

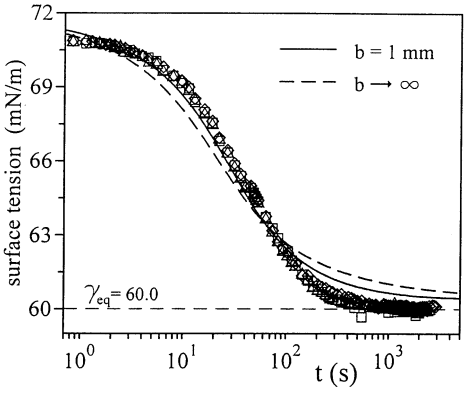

Fig. 12. A comparison between the dynamic surface tension data and the theoretical diffusion-controlled profiles from Frumkin (F_2) model at $C_\infty = 1.3 \times 10^{-8}$ mol cm^{-3} for a spherical interface ($b = 1$ mm, $D = 7.0 \times 10^{-6}$ cm^2 s^{-1}) and a planar interface ($D = 9.0 \times 10^{-6}$ cm^2 s^{-1}).

Acknowledgements

The authors thank Dr R. Miller and Professor E.V. Aksenenko for the IsoFit and WardTordai software packages and many helpful discussions. This work was supported by the National Science Council of Taiwan, Republic of China (NSC 89-2214-E-011-021).

References

[1] H. Diamant, D. Andelman, J. Phys. Chem. 100 (1996) 13732.
[2] H. Diamant, D. Andelman, Europhysics Lett. 34 (1996) 575.
[3] F. Ravera, L. Liggieri, A. Steinchen, J. Colloid Interface Sci. 156 (1993) 109.
[4] L. Liggieri, F. Ravera, A. Passerone, Colloids Surfaces A 114 (1996) 351.

[5] J. Eastoe, J.S. Dalton, P.G.A. Rogueda, E.R. Crooks, A.R. Pitt, E.A. Simister, J. Colloid Interface Sci. 188 (1997) 423.
[6] R. Miller, E.V. Aksenenko, L. Liggieri, F. Ravera, M. Ferrari, V.B. Fainerman, Langmuir 15 (1999) 1328.
[7] E.V. Aksenenko, A.V. Makievski, R. Miller, V.B. Fainerman, Colloids Surfaces A 143 (1998) 311.
[8] A.V. Makievski, D.O. Grigoriev, Colloids Surfaces A 143 (1998) 233.
[9] Y.C. Lee, Y.Y. Wang, M.W. Yang, H.S. Liu and S.Y. Lin, Effects of Temperature and Concentration on the Micellization of Nonionic Polyethoxylated Surfactants, submitted to J. Chin. Chem. Engr. (2002) in press.
[10] S.Y. Lin, K. McKeigue, C. Maldarelli, AIChE J. 36 (1990) 1785.
[11] S.Y. Lin, H.F. Hwang, Langmuir 10 (1994) 4703.
[12] Y.C. Lee, S.Y. Lin, H.S. Liu, Langmuir 17 (2001) 6196.
[13] R. Aveyard, D.A. Haydon, An Introduction to the Principles of Surface Chemistry, Cambridge University Press, Cambridge, 1973, Chapters 1 and 3.
[14] R.P. Borwankar, D.T. Wasan, Chem. Eng. Sci. 38 (1983) 1637.
[15] B. Li, G. Geeraerts, P. Joos, Colloids Surfaces 88 (1994) 251.
[16] S.Y. Lin, K. McKeigue, C. Maldarelli, Langmuir 10 (1994) 3442.
[17] J.K. Ferri, K.J. Stebe, J. Colloid Interface Sci. 209 (1999) 1.
[18] S.Y. Lin, R.Y. Tsay, L.W. Lin, S.I. Chen, Langmuir 12 (1996) 6530.
[19] H.C. Chang, C.T. Hsu, S.Y. Lin, Langmuir 14 (1998) 2476.
[20] R. Pan, J. Green, C. Maldarelli, J. Colloid Interface Sci. 205 (1998) 213.
[21] E.V. Aksenenko, Surfactants—chemistry, interfacial properties, applications, In: V.B. Fainerman, D. Möbius, R. Miller (Eds.), Studies in Interface Science, vol. 13, Elsevier, Amsterdam, 2001, Chapter 7.
[22] V.B. Fainerman, R. Miller, E.V. Aksenenko, A.V. Makievski, J. Krägel, G. Loglio, L. Liggieri, Adv. Colloid Interface Sci. 86 (2000) 83.
[23] Data of cloud point at 1.0 wt.% from Nikko Chemicals Co.
[24] R.B. Bird, W.E. Stewart, E.N. Lightfoot, Transport Phenomena, Wiley, New York, 1960, Chapter 16.
[25] D. Hayduk, W.D. Buckley, Chem. Engr. Sci. 27 (1972) 1997.
[26] R.Y. Tsay, S.Y. Lin, L.W. Lin, S.I. Chen, Langmuir 13 (1997) 3191.
[27] S.Y. Lin, H.C. Chang, E.M. Chen, J. Chem. Engr. Jpn. 29 (1996) 634.
[28] C.T. Hsu, C.H. Chang, S.Y. Lin, Langmuir 16 (2000) 1211.
[29] J.K. Ferri, S.Y. LinK.J. Stebe, J. Colloid Interface Sci. 241 (2001) 154.